Charge transfer dynamics of model charge transfer centers of a multicenter water splitting dye complex on rutile TiO2(110)

Matthew Weston, Andrew J. Britton, and James N. O'Shea

Citation: The Journal of Chemical Physics **134**, 054705 (2011); doi: 10.1063/1.3549573
View online: http://dx.doi.org/10.1063/1.3549573
View Table of Contents: http://scitation.aip.org/content/aip/journal/jcp/134/5?ver=pdfcov
Published by the AIP Publishing

Charge transfer dynamics of model charge transfer centers of a multicenter water splitting dye complex on rutile TiO_2(110)

Matthew Weston, Andrew J. Britton, and James N. O'Shea[a)]
School of Physics and Astronomy, and Nottingham Nanotechnology and Nanoscience Centre (NNNC), University of Nottingham, Nottingham NG7 2RD, United Kingdom

(Received 12 October 2010; accepted 11 January 2011; published online 2 February 2011)

Charge transfer dynamics between an adsorbed molecule and a rutile TiO_2(110) surface have been investigated in three organometallic dyes related to multicenter water splitting dye complexes: Ru 535 (*cis*-bis(isothiocyanato)bis(2,2′-bipyridyl-4,4′-dicarboxylato)-ruthenium(II)), Ru 455 (*cis*-bis(2,2′-bipyridyl)-(2,2′-bipyridyl-4,4′-dicarboxylic acid)-ruthenium(II)), and Ru 470 (tris(2,2′-bipyridyl-4,4′-dicarboxylic acid)-ruthenium(II)). The adsorption of the dye molecules on the rutile TiO_2(110) surface has been studied using core-level and valence photoemission. Dye molecules were deposited *in situ* using ultrahigh vacuum electrospray deposition. Core-level photoemission spectra reveal that each complex bonds to the surface via deprotonation of two carboxylic groups. All three dye complexes show evidence of ultrafast charge transfer to the TiO_2 substrate using the core-hole clock implementation of resonant photoemission spectroscopy. © *2011 American Institute of Physics*. [doi:10.1063/1.3549573]

I. INTRODUCTION

Dye-sensitized solar cells (DSCs) have become cost effective alternatives to photovoltaic silicon based solar cells.[1–3] The dye complexes used in DSCs are efficient light harvesting molecules and by adapting the structure of these molecules, it may be possible to create dye complexes capable of performing reactions using the energy from absorbed photons. Photosynthesis is a natural example of the application of absorbed light energy in a chemical reaction. A key process in photosynthesis is the water splitting reaction which produces electrons and hydrogen ions; these particles can then be used to create glucose molecules.[4] Ultimately the water splitting reaction produces hydrogen and oxygen molecules from water molecules using energy from absorbed sunlight. The reaction is essentially an energy transfer from the incident photon energy to chemical potential energy which can be used with more flexibility. This reaction can be reversed in a proton exchange membrane fuel cell (PEMFC) (Refs. 5 and 6) or the hydrogen can simply be combusted to release the chemical energy stored in the hydrogen molecules.

Dye-sensitized solar cells use dye molecules with extensive chromophores allowing for the efficient absorption of photons from the visible spectrum. Ru 535 (*cis*-bis(isothiocyanato)bis(2,2′-bipyridyl-4,4′-dicarboxylato)-ruthenium(II) also known as N3) is currently one of the most efficient dye complexes used in DSCs.[7] Its structure is shown in Fig. 1. The dye molecules are adsorbed onto the surface of a semiconductor with a wide bandgap such as TiO_2. Upon photoexcitation with visible light an electron in the adsorbed dye molecule is excited from the highest occupied molecular orbital (HOMO) to the lowest unoccupied molecular orbital (LUMO). Subsequently charge transfer from the adsorbed molecules to the surface can occur if the LUMO overlaps energetically with the conduction band of the substrate.

All of the molecules studied in this investigation contain one or more bi-isonicotinic acid ligands containing carboxylic acid groups which are capable of bonding to the TiO_2(110) surface as shown in Fig. 1. Previous studies of bi-isonicotinic acid adsorbed on rutile TiO_2(110) have shown that it bonds to the surface in a 2M-bidentate structure through deprotonation of its carboxylic acid groups.[8] Previous studies of Ru 535 on rutile TiO_2(110) using photoemission spectroscopy have also shown evidence of deprotonation of two carboxylic acid groups present on the bi-isonicotinic acid ligands.[9,10] The strong chemical coupling provided by this bonding geometry allows for efficient charge transfer between the LUMO and the conduction band of the substrate.

After successful charge transfer the adsorbed dye molecule would be left with a hole in its HOMO. In photovoltaic DSCs the hole can be filled by electrons coming from either a liquid electrolyte or an adsorbed layer of gold on the substrate.[11,12] In a water splitting photoelectrochemical cell the hole is replaced by electrons from the water molecule during the reaction. This process competes with other electron replenishment channels and therefore back transfer of electrons would need to be minimized for an efficient water splitting dye complex. The ability of gold surfaces to transfer electrons to adsorbed molecules would suggest that gold is not a suitable substrate for a water splitting device.[12–14] Titanium dioxide, on the other hand, shows only efficient charge transfer from the molecule to the substrate and is therefore an ideal candidate. Any electrons transferred to the substrate are transported to the cathode where they combine with hydrogen ions produced during the water splitting reaction to create hydrogen molecules which can be used as fuel. The reaction has previously been performed using both single and multicenter

a)Electronic mail: james.oshea@nottingham.ac.uk.

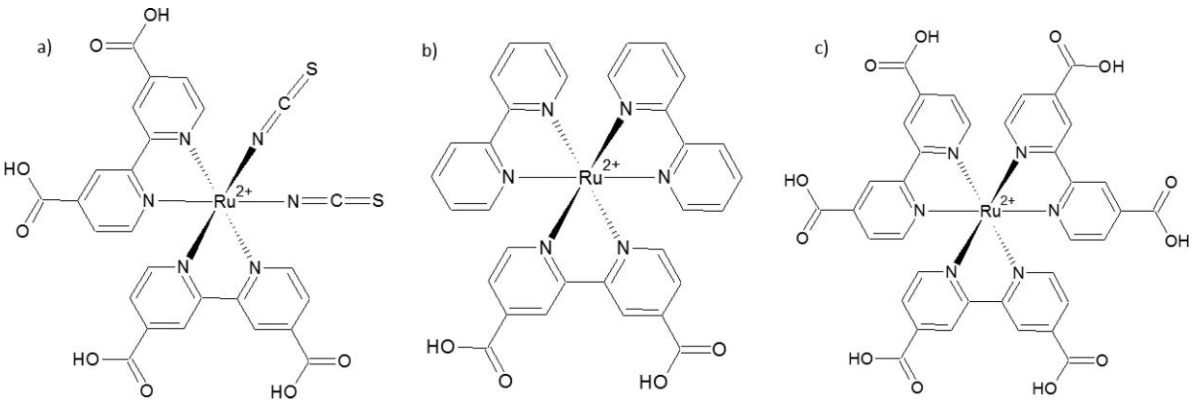

FIG. 1. Chemical structures of the Ru 535 molecule (a), Ru 455 molecule (b), and Ru 470 molecule (c).

ruthenium dye molecules as catalysts both on surfaces and in solution.[15–17]

Previous studies have shown that a multicenter ruthenium dye complex performs the water splitting reaction more efficiently than a single center complex.[17] The systems studied in this work are models of the charge transfer center of such a multicenter water splitting complex. The dye complexes Ru 535 and two closely related dyes, Ru 455 (*cis*-bis(2,2′-bipyridyl)-(2,2′-bipyridyl-4,4′-dicarboxylic acid)-ruthenium(II)) and Ru 470 (tris(2,2′-bipyridyl-4,4′-dicarboxylic acid)-ruthenium(II)) were adsorbed onto a rutile TiO_2(110) substrate. The dye molecules were deposited *in situ* at monolayer and multilayer coverages using UHV electrospray deposition. This technique has been used successfully in previous studies to deposit carbon nanotubes,[18] C_{60} molecules,[19,20] zinc protoporphyrin,[21] polymers,[22] biomolecules,[23] and the Ru 535 dye complex.[9,24]

The adsorbed dye molecules were studied using X-ray photoemission spectroscopy (XPS), near-edge X-ray absorption fine structure (NEXAFS) spectroscopy, and resonant photoemission spectroscopy (RPES) in order to observe their bonding, electronic structure, and charge transfer dynamics.

II. METHOD

Experiments were carried out at the undulator beamline I311 at MAX-lab, Sweden.[25] The I311 end station is equipped with a Scienta SES-200 electron analyzer.

The experiments were performed using a single crystal rutile TiO_2(110) substrate of dimensions 10 mm × 10 mm × 1 mm (Pi-Kem, UK), mounted on a pyrolytic boronitride heater which allowed for *in situ* annealing of the sample. Cycles of sputtering using 2 and 1 keV Ar^+ ions, and annealing in UHV to ∼600 °C, were used to prepare the surface. Initially, repeated cycles of sputtering and annealing were performed in order to change the crystal from an insulator to an *n* type semiconductor through the introduction of bulk defects necessary to avoid sample charging. These defects, which also turn the crystal slightly blue, were minimized at the surface through annealing as described above, but nevertheless can frequently be observed as a density of states just below the conduction band edge in the valence band photoemission spectra. The substrate was deemed clean when it showed a negligible C 1*s* core-level signal and a single Ti^{4+} oxidation state in the Ti 2*p* spectrum.

The dye molecules (Solaronix SA, Switzerland) were deposited using an *in situ* UHV electrospray deposition source (MolecularSpray, UK), from a solution of ∼5 mg of dye in 200 ml of a 3(methanol):1(water) mixture. The apparatus used and the process by which the molecules are taken from *ex situ* solution to *in situ* vacuum are described in detail elsewhere.[9] In summary, the liquid is pushed through a hollow stainless steel needle held at ∼2 kV. Here, the liquid becomes ionized and a jet emerges consisting of multiply charged droplets. The jet enters vacuum through a series of differentially pumped chambers, in which the droplets lose solvent through evaporation, and split repeatedly due to Coulomb repulsion. Between depositions, the electrospray system was sealed off from the preparation chamber using an UHV gate valve. With the valve open but the needle voltage turned off and thus no electrospray process occurring, the pressure in the preparation chamber was $\sim 2 \times 10^{-8}$ mbar. With the voltage turned on, the preparation chamber pressure rose to $\sim 5 \times 10^{-7}$ mbar, the additional pressure being due to residual solvent molecules in the beam.

For the electron spectroscopy data, the total instrument resolution ranges from 65 to 195 meV. All XPS spectra have been calibrated to the substrate O 1*s* peak at 530.05 eV,[26] and a Shirley background removed before curve fitting using Voigt functions. NEXAFS and RPES spectra were taken over the N 1*s* absorption edge and were measured using the electron analyzer. For NEXAFS spectra the nitrogen Auger yield was used while for RPES spectra the valence band photoemission was monitored. For all measurements, the sample was swept continuously at a rate of at least 1.25 μm/s, following beam damage studies to determine a safe exposure time.

Density functional theory (DFT) simulation calculations were carried out as an aid to interpret the experimental data. Geometry optimizations were performed on free molecules of each dye complex using Dmol^3 at the DFT-generalized gradient approximation level (DFT-GGA) with the Perdew–Burke–Enzerhof (PBE) functional.[27–29] The optimized structures were then used to calculate the molecular orbitals for each molecule.

III. RESULTS AND DISCUSSION

A. Adsorption

The samples used for the following spectra are classed as either *monolayer* or *multilayer*. Here, a monolayer is defined as a sample having the vast majority of molecules directly adsorbed to the surface and a multilayer is defined as having a film of molecules thick enough that the majority of photoelectrons in XPS come from molecules above the first adsorbed layer. Using the O 1*s* XPS spectra the multilayer is estimated to be approximately two to three layers thick for each dye complex. The binding energies (BEs) of the peaks discussed are summarized in Table I.

Figure 2 shows the O 1*s* monolayer spectra of each dye complex on rutile TiO_2(110). For all three dye molecules the spectrum is dominated by the TiO_2 substrate oxygen peak. The two smaller peaks are due to the oxygen atoms in the carboxylic acid groups of the bi-isonicotinic acid ligands of each molecule. For isolated dye molecules the intensity of these two peaks should be equal due to the equivalent number of carbonyl (C=O) and hydroxyl (C–OH) oxygen atoms.

Previous studies of bi-isonicotinic acid and Ru 535 have shown deprotonation of the hydroxyl groups on adsorption to TiO_2 to form a 2M-bidentate structure.[8,9] This is a common bonding arrangement for pyridine based molecules with carboxylic acid groups on the TiO_2 surface.[30–32] Ru 535 is thought to bind to the surface using a single bi-isonicotinic acid ligand.[9] After deprotonation the two oxygen atoms share an electron and are chemically equivalent. The BE of this oxygen species is similar to that of the carbonyl oxygen atom in isolated molecules, and the two groups are unresolvable in the XPS spectra.[8] In Fig. 2 the monolayer COO^-/C=O:C–OH intensity ratio is approximately 3:1 for Ru 535 and 2:1 for Ru 470. There is no evidence of a hydroxyl oxygen peak in the Ru 455 spectrum. Assuming that all molecules of a dye complex bond to the surface in an equivalent way, these results are similar to those expected if two carboxylic acid groups of each dye complex are bonded to the surface. The expected ratios from this bonding geometry would be 3:1 for Ru 535 and 2:1 for Ru 470, and no hydroxyl peak for the Ru 455 complex, in direct agreement with the experimental results. This shows that each molecule bonds to the surface using two carboxylic acid groups which provides information on the binding geometry of each complex. Ru 455 can only bond to the surface using both of the carboxylic acid groups on its lone bi-isonicotinic acid ligand whereas Ru 470 can bond to the surface using either both of the carboxylic acid groups on a single bi-isonicotinic acid ligand or a single carboxylic acid group from each of the two bi-isonicotinic acid ligands. Previous experiments have shown that Ru 535 has an additional bond to the TiO_2 surface through the sulfur atom of one of its isothiocyanate groups;[9] however, the other two dye complexes do not contain isothiocyanate groups, so they are incapable of bonding in this fashion.

TABLE I. BEs (eV) for monolayers of each molecule calibrated to the substrate O 1*s* peak at 530.05 eV.

		Ru 535	Ru 455	Ru 470
PES				
O 1*s*	TiO_2	530.05	530.05	530.05
	C=O and COO^-	531.2	531.2	531.1
	C–OH	532.3	...	532.3
C 1*s*	Pyridine	285.0	285.6	285.4
	Thiocyanate	286.0	...	...
	Carboxyl	287.8	288.1	288.0
Ru 3*d*		280.6	281.1	281.0
N 1*s*	Thiocyanate	397.6	...	...
	Pyridine	399.7	400.4	400.1
Valence band	HOMO	1.3	1.85	1.9
N 1*s* NEXAFS				
Unshifted	LUMO	0.1	0.8	0.5
Aligned to optical data	LUMO	−1.1	−0.9	−0.75

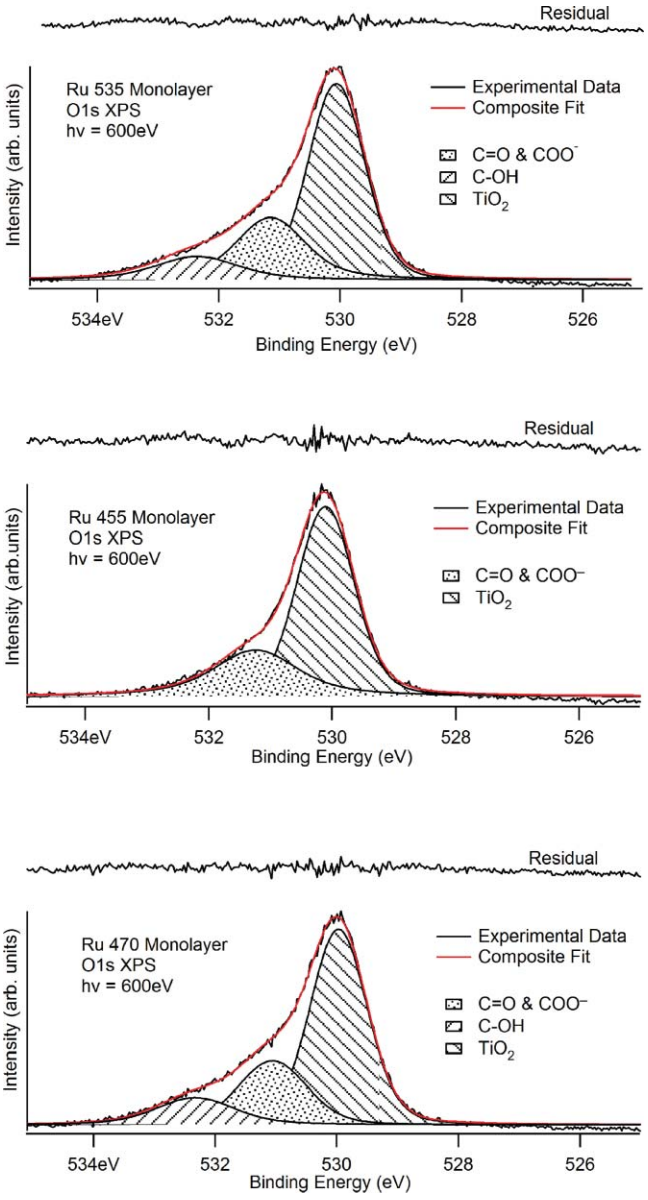

FIG. 2. O 1*s* core-level photoemission spectra of monolayers of Ru 535 (top), Ru 455 (middle), and Ru 470 (bottom) on rutile TiO_2(110), measured using $h\nu = 600$ eV.

Figure 3 shows O 1*s* XPS spectra of multilayers of each dye complex. The multilayer spectrum of the Ru 535 molecule shows the expected intensity ratio of 1:1 for the C=O:C–OH oxygen peaks, which is in agreement with results reported previously.[9] The spectrum for Ru 455 appears to show evidence of deprotonation already in the multilayer from the reduced intensity of the C–OH signal. This is likely due to some hydrogen loss from the dye complex to the PF_6^- counter ions present in the deposition solution. The multilayer spectrum for Ru 470 shows the expected intensity ratio of 1:1; however, an additional peak is visible in the spectrum at higher BE than the C–OH peak. This feature is most likely due to intermolecular hydrogen bonds between the bi-isonicotinic acid ligands of the dye molecules in the multilayer.[30]

Figure 4 shows the C 1*s* and Ru 3*d* XPS spectra of monolayers of each dye complex. The spectra look similar for each molecule with the exception of an additional peak in the Ru 535 spectrum due to the carbon atoms present in the isothiocyanate groups. Each spectrum is dominated by a peak due to the carbon atoms in pyridine groups. Also present at higher BE is the peak due to the carbon atom in the carboxylic acid groups. There are also two peaks due to the central ruthenium ion as the Ru 3*d* state is a doublet state with a spin orbit splitting of 4.2 eV.[33] The lower BE Ru $3d_{5/2}$ peak is present at 281 eV. This is approximately 1 eV higher than metallic ruthenium,[33] which is consistent with the Ru^{2+} oxidation state of the metal center. This strongly suggests that the molecules have retained their molecular integrity during deposition.

Figure 5 shows the N 1*s* XPS spectra of monolayers of each dye complex. The Ru 535 molecule shows two peaks due to the nitrogen atoms in its pyridine and thiocyanate groups, in agreement with previously reported results.[9] The Ru 455 dye

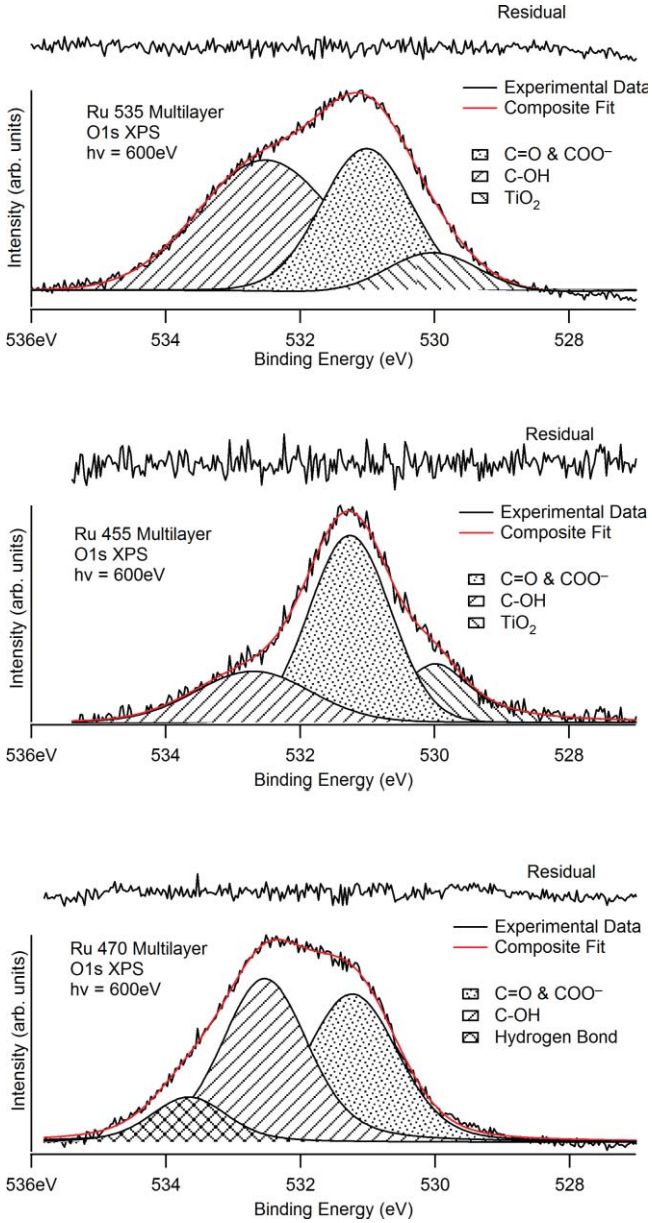

FIG. 3. O 1*s* core-level photoemission spectra of multilayers of Ru 535 (top), Ru 455 (middle), and Ru 470 (bottom) on rutile TiO_2(110), measured using $h\nu = 600$ eV.

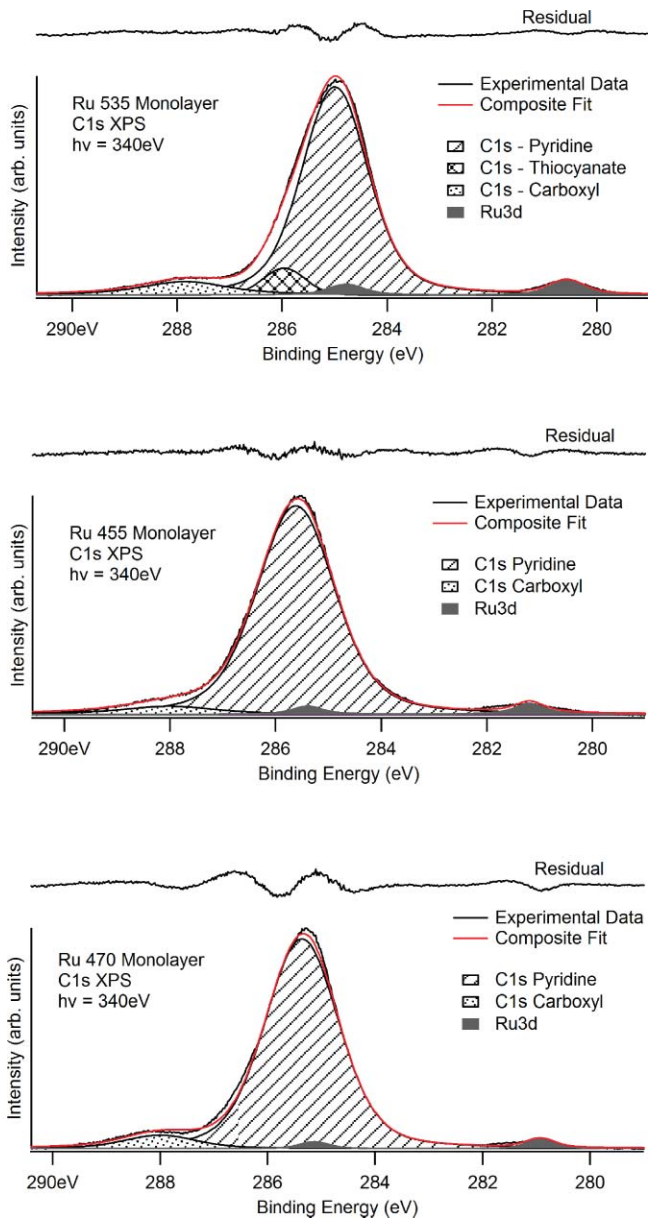

FIG. 4. C 1*s* and Ru 3*d* core-level photoemission spectra of monolayers of Ru 535 (top), Ru 455 (middle), and Ru 470 (bottom) on rutile TiO_2(110), measured using $h\nu = 340$ eV.

complex shows only a single nitrogen peak as expected from its chemical structure. Ru 470 not only exhibits a single peak reflecting the structure of the molecule but also a low binding energy tail, possibly due to a small amount of impurities in the deposition solution.

B. Electronic structure

In a DSC, electrons are photoexcitated from high-lying occupied molecular orbitals to previously unoccupied molecular orbitals. For subsequent electron injection into the substrate, the unoccupied level in question must overlap with available states in the substrate conduction band. Spectra representing the occupied and the unoccupied states of monolayers of each dye complex have here been placed on a common BE scale as shown in Fig. 6, following a procedure outlined elsewhere.[34] This procedure has previously been performed on a monolayer of Ru 535.[9] The resulting energy level alignment diagrams can be used to identify the potential charge transfer processes that can occur in the model charge transfer centers.[14,35–37]

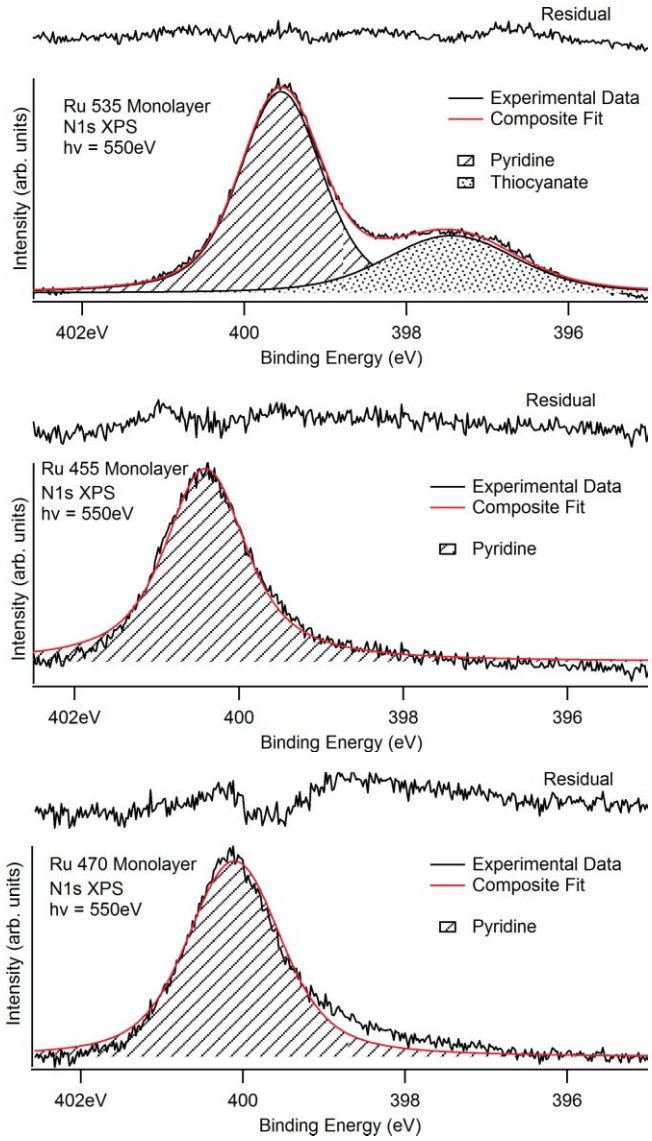

FIG. 5. N 1*s* core-level photoemission spectra of monolayers of Ru 535 (top), Ru 455 (middle), and Ru 470 (bottom) on rutile TiO_2(110), measured using $h\nu = 550$ eV.

Figure 6 shows the N 1*s* (Auger yield) NEXAFS and valence photoemission spectra for a monolayer of each dye complex, along with the clean substrate valence photoemission spectrum (measured at $h\nu$=110 eV). The N 1*s* core-level spectra of monolayers of all the three dye complexes are dominated by the pyridine N peak; therefore, this peak was used to place the NEXAFS on the common BE axis. Previous studies on the bi-isonicotinic acid ligand and on the Ru 535 dye complex have shown that the N 1*s* NEXAFS is dominated by pyridinelike π^* orbitals.[9,38,39]

The lowest binding energy peak in the valence photoemission spectra corresponds to the HOMO. For each dye complex the HOMO is present within the substrate bandgap which prevents back transfer of electrons from the substrate. The HOMO is located at a BE of 1.85 and 1.90 eV for the Ru 455 and Ru 470 dye complexes, respectively. The HOMO of both Ru 455 and Ru 470 dye complexes is located at higher BE than that of the Ru 535 (1.3 eV). After charge transfer from the molecules to the substrate has occurred this could create a larger potential to remove electrons from an attached water molecule. Optical absorption spectra of the dye complexes show maxima, which correspond to photon energies that photoexcite electrons from the HOMO to various unoccupied levels. The lowest in energy of these maxima is attributed to the HOMO → LUMO transition corresponding to a Ru(4d) → bpy(π^*)COOH transition.

In the present case, where the unoccupied states are probed using N 1*s* NEXAFS, a *core* exciton (bound electron–hole pair) is created, whereas in an optically excited system, a *valence* exciton is created. The presence of a hole in both NEXAFS and optical absorption shifts the unoccupied states to higher binding energy with respect to the ground state. The BE of the excitons, equivalent to the amount by which the unoccupied levels shift, is attributed to a combination of the Coulomb interaction between the hole and the excited electron and the rehybridization of the molecular states upon core- or valence-hole creation.[40] Comparing the HOMO–LUMO gap for optical excitation (2.3, 2.73, and 2.65 eV) to the HOMO–LUMO gap for the core-excited system (1.2, 1.1, and 1.4 eV), the difference in energy is 1.1, 1.6, and 1.3 ± 0.1 eV for the Ru 535, Ru 455, and Ru 470 dye complexes, respectively. This is indicative of the difference between the N 1*s* core exciton and valence exciton BEs for the molecules. These values are consistent with the difference in BE found for pyridine,[40] a molecule closely related to the bi-isonicotinic acid ligands of the dye complexes especially concerning the chemical environment of the nitrogen atoms being probed here.

Shifting the NEXAFS spectra of each dye complex into line with the optical HOMO–LUMO gap, as shown in Fig. 6, causes the LUMO to lie above the conduction band edge. In a real solar cell or water splitting device this energetic overlap permits electron injection from the LUMO into the substrate for both dye complexes. The presence of a core exciton in the NEXAFS causes the LUMO of the core-excited systems to lie within the substrate bandgap preventing charge transfer

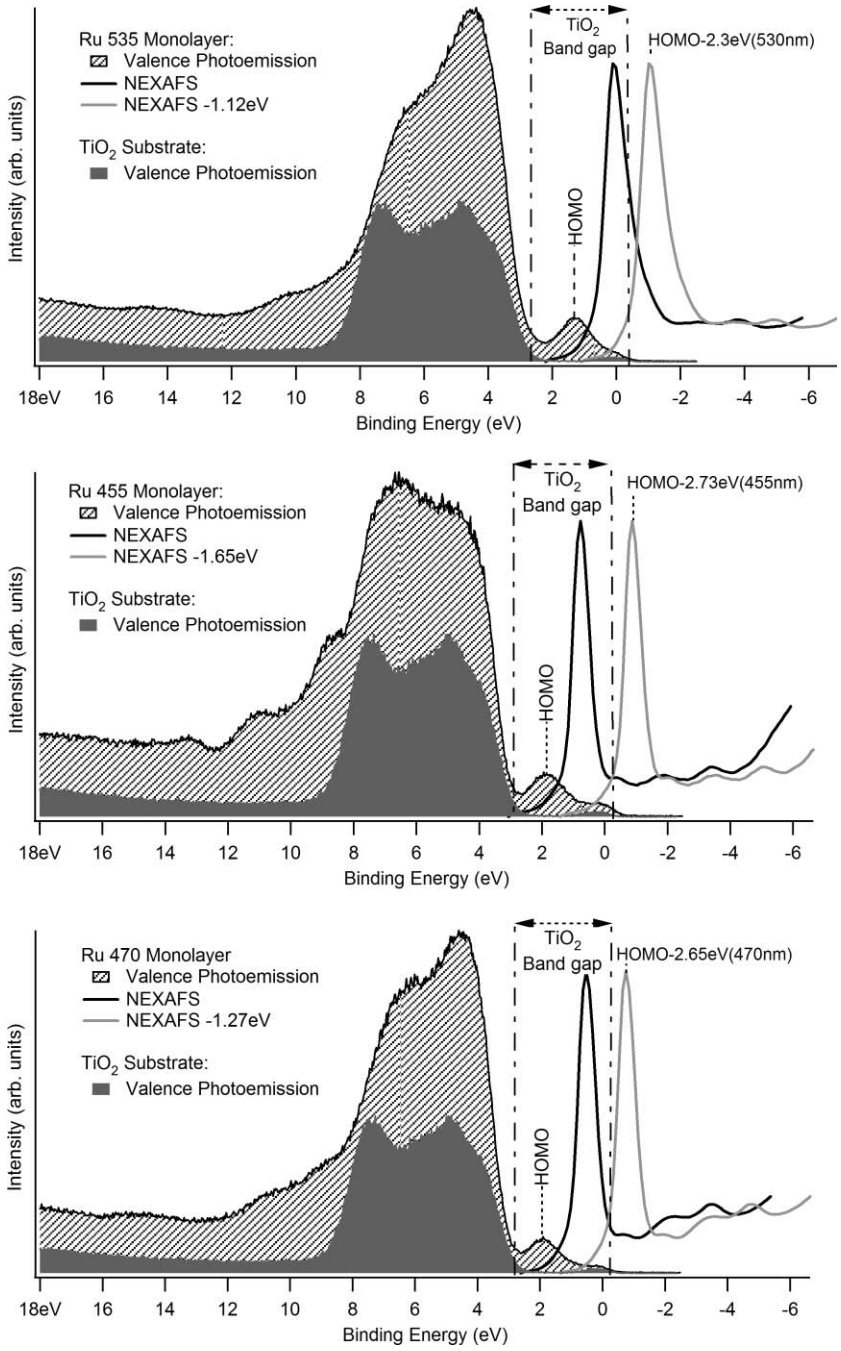

FIG. 6. Valence band photoemission spectra of the clean substrate and of a monolayer of dye molecule, adjacent to a N 1*s* NEXAFS spectrum of the monolayer. The NEXAFS spectra are also shown shifted to align with the relevant optical HOMO–LUMO gap (shown in a lighter shade and labeled with the position of the measured HOMO minus the energy of the optical absorption). The photoemission spectra were measured using $h\nu = 60$ eV. The NEXAFS spectra were taken over the photon energy range $h\nu = 397$–406 eV.

for this orbital. In Sec. III C, electrons excited to the LUMO are used as a reference, allowing us to probe electron injection from those remaining unoccupied levels that lie above the conduction band edge.[36,41]

C. Charge transfer dynamics

In water splitting DSCs the initial step of the reaction is electron injection from the excited molecule into the substrate conduction band. RPES is used here to investigate molecule-to-substrate charge transfer. This technique enables us to quantify the delocalization of charge from unoccupied molecular orbitals to the substrate on the low femtosecond time scale, previously demonstrated for the bi-isonicotinic acid ligand and the Ru 535 molecule on TiO_2(110).[9,36]

The core-hole clock implementation of RPES uses the fact that if charge transfer is occurring, it must be competing with the deexcitation of the excited state via resonant photoemission or resonant Auger. The time taken for deexcitation here can also be described as the lifetime of the N 1*s* core-hole. Here we calculate the electron injection time from the LUMO+2 and LUMO+3 of each dye complex where

possible. The electron injection time τ_{EI} for electrons moving from the unoccupied level of the molecule adsorbed to the substrate to the unoccupied substrate states is given by Eq. (1). For a complete discussion of the core-hole clock implementation of RPES, including the derivation of this equation, the reader is directed to Brühwiler *et al.*[41] and references therein.

$$\tau_{EI} = \tau_{CH} \frac{I^{mono}_{RPES}/I^{mono}_{NEXAFS}}{I^{multi}_{RPES}/I^{multi}_{NEXAFS} - I^{mono}_{RPES}/I^{mono}_{NEXAFS}} \quad (1)$$

The variables I^{mono}_{RPES} and I^{multi}_{RPES} represent the intensities of the unoccupied peak being studied in the monolayer and multilayer, respectively. These values are each normalized by the total cross sections as provided by the NEXAFS intensities I^{mono}_{NEXAFS} and I^{multi}_{NEXAFS}. The variable τ_{CH} is the average N 1*s* core-hole lifetime which has been measured as 6 fs.[42]

As discussed in Sec. III B the LUMO of each molecule lies energetically within the substrate band-gap, so the injection of an electron excited to this level into the substrate conduction band is energetically forbidden. Charge injection of excited electrons is however energetically allowed from other unoccupied molecular orbitals that overlap with the conduction band of the substrate. The experimental RPES data includes Auger peaks which need to be excluded from the charge transfer analysis, this is achieved by integrating over a selected BE window as shown in Fig. 7 for both the multilayer and monolayer. Any peaks at the energies of the LUMO+2 and LUMO+3 resonances are due solely to resonant photoemission, as normal photoemission contributes a sloping background only. The LUMO+1 is not considered, as it cannot be separated from the LUMO.

The RPES spectra are normalized to the intensity of the LUMO, as are the corresponding NEXAFS spectra which are also shown in Fig. 8. In the NEXAFS spectra, the peaks represent the unoccupied levels' full intensities, whereas for RPES, the LUMO has its full intensity but the other unoccupied levels may be depleted by charge transfer. For the multilayer, it can be seen that the LUMO+2 and LUMO+3 peaks are smaller in the RPES than in the NEXAFS. Since no charge transfer to the substrate can occur in the multilayer, this intensity reduction is attributed purely to matrix element effects due to the different techniques used.[37] For the monolayer RPES the peaks have been reduced further, in some cases down to the level of noise, indicating that charge transfer is occurring from these levels on the timescale of the core-hole lifetime.

The multilayer RPES spectrum of Ru 535 in Fig. 8 shows a very broad LUMO peak compared to the multilayer RPES spectra of the Ru 455 and Ru 470 molecules. This has been attributed to overlapping signals coming from the two different types of nitrogen atoms found in Ru 535. In Ru 455 and Ru 470 there is only a single major chemical environment for the nitrogen atoms. In the Ru 455 and Ru 470 multilayer RPES spectra it is possible to see a distinct LUMO+1 peak, which is not possible in the Ru 535 spectrum due to the broad peak.

For the Ru 535 and Ru 455 monolayer RPES peaks there is no discernable peak at the same BE as the corresponding peak in the NEXAFS spectrum. For these peaks the level of noise is taken as an upper limit for the intensity of any peak that might be present. This is then used to calculate an upper limit for the charge transfer time according to Eq. (1), shown for each molecular orbital studied in Table II. These values are in agreement with the upper limit on the time scale for charge transfer of both Ru 535 and the bi-isonicotinic acid ligand on TiO_2, which have previously been found to be 16 and 3 fs, respectively.[9,36] The reduction of the Ru 535 LUMO+3 upper limit on the charge transfer timescale is attributed to a better signal-to-noise ratio in the current experiment. The Ru 455 and Ru 470 dye complexes show charge transfer timescales on the same order of magnitude as the Ru 535 complex; however, all of the orbitals studied in these complexes appear to have slower charge transfer timescales than the Ru 535 LUMO+3. The Ru 470 complex appears to be the least efficient at charge transfer; this could be explained if the Ru 470 complex adopts a different bonding geometry on the rutile TiO_2(110) surface compared to the Ru 535 and Ru 455 complexes. Ru 535 is thought to bond to the rutile TiO_2(110) surface using both of the carboxylic acid groups on a single bi-isonicotinic acid ligand,[9] Ru 455 must also adopt this method

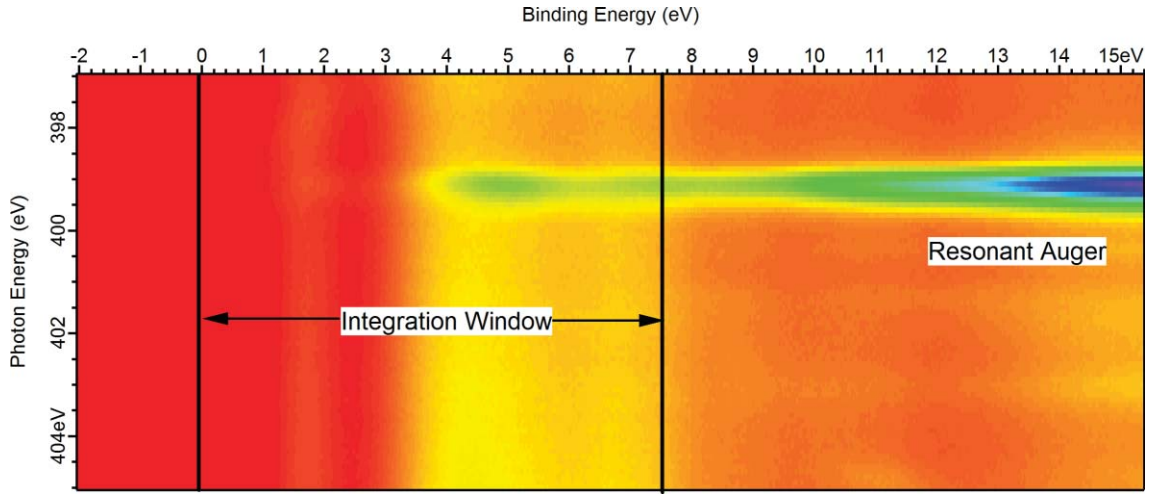

FIG. 7. N 1*s* RPES spectrum of a monolayer of Ru 470 on rutile TiO_2(110) showing the BE integration window used to remove the Auger peaks.

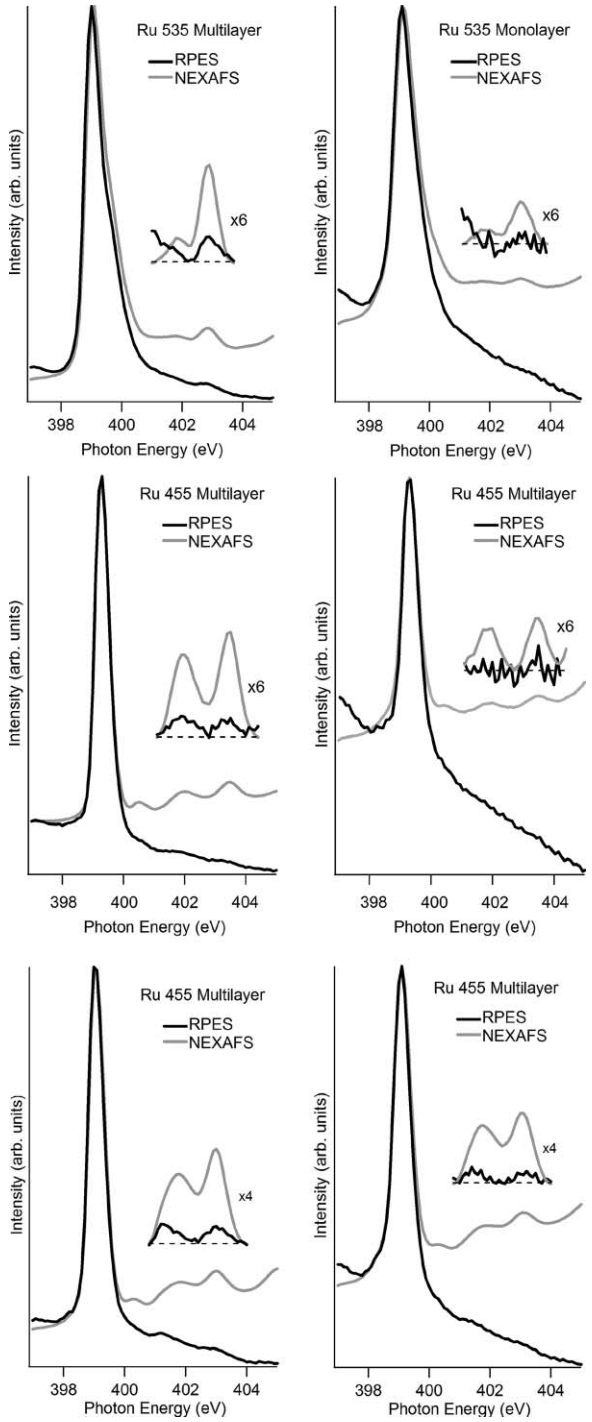

FIG. 8. N 1*s* RPES and N 1*s* NEXAFS spectra of multilayers (left) and monolayers (right) of Ru 535 (top row), Ru 455 (middle row), and Ru 470 (bottom row). The RPES spectra are BE integrations over a range which excludes the Auger peaks. Also shown are magnifications of the LUMO+2 and LUMO+3 regions.

because of having a single bi-isonicotinic acid ligand.[9] Ru 470 could possibly bond to the surface using a carboxylic acid group from each of the two different bi-isonicotinic acid ligands, this geometry may be less efficient for charge transfer as it may not provide as much chemical coupling to the surface as the geometry adopted for Ru 535 and Ru 455.

Various different experimental techniques have previously been used to study Ru 535 on TiO_2 such as laser pump–probe techniques which have found instrument limited charge transfer timescales of 50 fs (Refs. 43 and 44). DFT simulations have also been performed on this system examining the charge transfer process which predict charge transfer time scales on the order of 10 fs.[45] The results for the charge transfer timescale for the molecules studied in these experiments are consistent with the results obtained from these other types of experiments.

The $I^{\text{multi}}_{\text{RPES}}/I^{\text{multi}}_{\text{NEXAFS}}$ ratio can be reduced by ultrafast delocalization of electrons within the molecule; this process leads to a reduction in the resonant photoemission signal even in the absence of charge transfer to the substrate. Evidence of ultrafast intramolecular delocalization has previously been observed in the RPES spectra of a ruthenium complex comprised of three bipyridine ligands, for which little or no resonant photoemission was observed for resonances lying higher than the LUMO in the multilayer.[46] The lowering of the $I^{\text{multi}}_{\text{RPES}}/I^{\text{multi}}_{\text{NEXAFS}}$ ratio is therefore attributed to a combination of the matrix element effect and ultrafast intramolecular delocalization. For the monolayer, a fraction of the remaining localized electrons are capable of undergoing charge transfer into the substrate; this reduces the RPES/NEXAFS ratio further, and this reduction can be measured to gain insights into the charge transfer process. Intramolecular delocalization is accounted for in Eq. (1) through the experimentally derived value of $I^{\text{multi}}_{\text{RPES}}/I^{\text{multi}}_{\text{NEXAFS}}$.

The energy alignment diagrams in Fig. 6 show that the LUMO of each of the dye complexes is capable of charge transfer when the dye is excited using visible light. The creation of a core-hole in RPES prevents the LUMO from being studied directly due to the LUMO lying within the TiO_2 band-gap in the core-excited system. However, the LUMO, LUMO+2, and LUMO+3 of each dye complex are all thought to be located on the bi-isonicotinic acid ligands. Therefore, it can be assumed that the coupling of these orbitals to the substrate and, therefore, the corresponding charge transfer dynamics will be similar.

For resonant photoemission to occur following core excitation, the occupied and unoccupied orbitals involved must have some interaction. The largest probability for resonant photoemission occurs when both of the electrons involved in the transition are located on the same atom, specifically the site of the core-hole. Resonant photoemission is in essence a special type of Auger decay and while interatomic Auger transitions can occur,[47] the rates of these events are negligible in all but the lowest energy Auger processes. In Ru 535 state-dependent resonant enhancements are observed,[9] providing evidence that the LUMO and LUMO+1 are located on different parts of the molecule. In the previous work the LUMO was attributed to the bi-isonicotinic acid ligands and the LUMO+1 to the thiocyanate ligands, DFT simulations were performed on the Ru 535 molecule which provided further evidence for this conclusion.[9] In the Ru 455 and Ru 470 dye complexes there is no evidence of significant state-dependent resonant enhancements, suggesting that the LUMO and LUMO+1 of each dye complex have similar spatial distributions. The DFT simulations of the Ru 455 and Ru 470 dye

TABLE II. Table of RPES/NEXAFS ratios for multilayer and monolayer coverages of dye molecules and the calculated upper limit on charge transfer timescale for each orbital studied.

Dye molecule	Orbital	Multilayer RPES/NEXAFS ratio	Monolayer RPES/NEXAFS ratio	Upper limit on charge transfer timescale (fs)
Ru 535	LUMO+3	0.259	0.170	12
Ru 455	LUMO+2	0.252	0.190	18
Ru 470	LUMO+2	0.198	0.155	21
Ru 470	LUMO+3	0.168	0.124	17

complexes have shown that the HOMO of each dye complex is located on the central ruthenium atom and that the LUMO of each dye complex is located on its bi-isonicotinic acid ligands as shown in Fig. 9.

In these experiments resonant photoemission requires some degree of overlap between the HOMO, LUMO, and the core-excited atom; however, in a real DSC only an overlap between the HOMO and LUMO is required for photoexcitation between the states. Figure 9 shows that the calculated HOMO and LUMO of the Ru 455 dye complex have some overlapping spatial distribution on the central ruthenium metal ion which facilitates photoexcitation between the two orbitals. The Ru 470 dye complex appears to show very little overlap between the calculated HOMO and LUMO orbitals which may reduce the efficiency of this dye complex as a DSC.

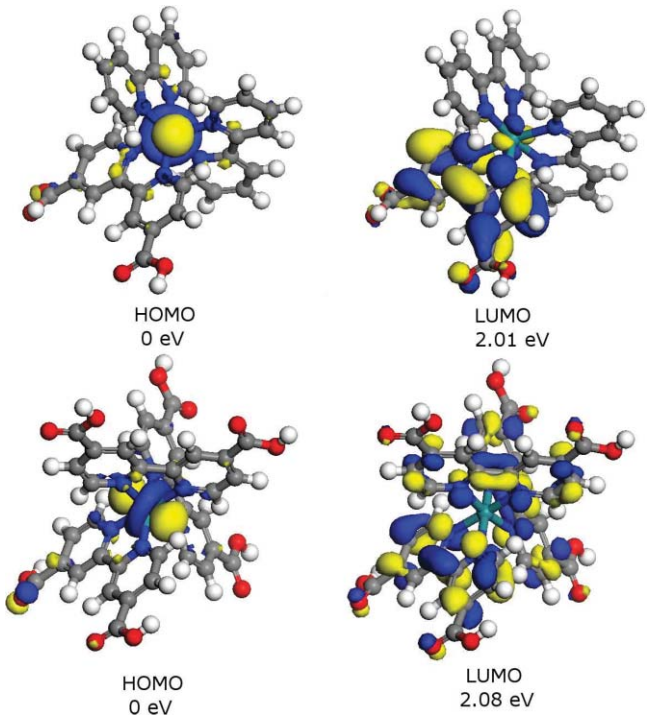

FIG. 9. DFT calculations showing electron orbitals of a geometry-optimized free Ru 455 molecule (top) and Ru 470 molecule (bottom) together with calculated orbital energies.

IV. CONCLUSIONS

UHV electrospray deposition has been used to deposit monolayers and multilayers of Ru 455, Ru 535, and Ru 470 dye complexes on the rutile TiO_2(110) surface *in situ*. Photoemission spectroscopy has been used to characterize the core and valence levels of the system, which were used to deduce the bonding geometry of each dye complex on the rutile TiO_2(110) surface. We find that for both dye complexes two carboxylic acid groups deprotonate so that their O atoms bond to Ti atoms of the substrate surface.

The energetic alignment of the system was determined by placing the valence photoemission and N 1*s* NEXAFS of a monolayer of each dye complex onto a common BE scale. The bandgap of TiO_2(110) was aligned using the valence photoemission of the clean substrate. The optical absorption maximum for each dye complex was attributed to the HOMO $\rightarrow$ LUMO transition in a working solar cell. This was used to compare the energetics as they would appear for photoexcitation from the valence band (as occurs in working DSCs) with those found for photoexcitation from the N 1*s* core-level, for which the unoccupied levels appear at higher BE. This comparison allowed quantification of the difference in BE of a core and valence excitation for each dye complex system, found to be 1.6 and 1.3 $\pm$ 0.1 eV. for the Ru 455 and Ru 470 dye complexes, respectively.

The core-hole clock implementation of RPES was used to find that electron injection from the LUMO+2 and LUMO+3 of each dye complex to the substrate occurs in the range of 12–21 fs for the orbitals studied here. In agreement with previous studies of Ru 535, bi-isonicotinic acid and related molecules on TiO_2, which found charge transfer to occur on the femtosecond timescale. It is thought that the studied orbitals and the LUMO of each dye complex are all located on the bi-isonicotinic acid ligands, so electron injection in valence excited systems is expected to occur in a similar time scale. The Ru 470 monolayer RPES peaks are still clearly visible suggesting that this dye complex is the least efficient molecule at charge transfer studied here.

The valence band photoemission spectra show that the HOMO of the Ru 455 and Ru 470 dye complexes occur at lower BE than that of the Ru 535 dye complex. The difference between the BEs is attributed to the difference in electron densities on the central ruthenium ion, which is caused by the difference in electronegativity of the attached ligands. In a water splitting dye complex the potential to remove electrons

from a water molecule is created by a hole in the HOMO. Having a HOMO at lower BE causes a larger potential which should be more effective at removing electrons from the water molecule. The information obtained from these experiments will be used in the design of a multicenter water splitting DSC.

ACKNOWLEDGMENT

We are grateful for the financial support by the European Community—Research Infrastructure Action under the FP6 "Structuring the European Research Area" Programme (through the Integrated Infrastructure Initiative "Integrating Activity on Synchrotron and Free Electron Laser Science"), the UK Engineering and Physical Sciences Research Council (EPSRC). We express our thanks to the staff of MAX-lab for their technical assistance, especially to Dr. K. Schulte and also to Dr. J. Schnadt of the Division of Synchrotron Radiation Research, Lund University.

[1] M. Grätzel and A. Hagfeldt, Acc. Chem. Res. **33**, 269 (2000).
[2] M. Grätzel, Nature **414**, 338 (2001).
[3] M. Grätzel, J. Photochem. Photobiol. C **4**, 145 (2003).
[4] A. Magnuson, M. Anderlund, O. Johansson, P. Lindblad, R. Lomoth, T. Polivka, S. Ott, K. Stensjö, S. Styring, V. Sundström, and L. Hammarström, Acc. Chem. Res. **42**, 1899 (2009).
[5] P. Costamagna and S. Srinivasan, J. Power Sources **102**, 242 (2001).
[6] P. Costamagna and S. Srinivasan, J. Power Sources **102**, 253 (2001).
[7] M. Grätzel, J. Photochem. Photobiol. A **164**, 3 (2004).
[8] L. Patthey, H. Rensmo, P. Persson, K. Westermark, L. Vayssieres, A. Stashans, Å. Petersson, P. A. Brühwiler, H. Siegbahn, S. Lunell, and N. Mårtensson, J. Chem. Phys. **110**, 5913 (1999).
[9] L. C. Mayor, J. B. Taylor, G. Magnano, A. Rienzo, C. J. Satterley, J. N. O'Shea, and J. Schnadt, J. Chem. Phys. **129**, 114701 (2008).
[10] E. M.J. Johansson, M. Hedlund, H. Siegbahn, and H. Rensmo, J. Phys. Chem. B **109**, 22256 (2005).
[11] M. Grätzel, Nature **421**, 586 (2003).
[12] E. W. McFarland and J. Tang, Nature **421**, 616 (2003).
[13] A. J. Britton, A. Rienzo, K. Schulte, and J. N. O'Shea, J. Chem. Phys. **133**, 094705 (2010).
[14] J. B. Taylor, L. C. Mayor, J. C. Swarbrick, J. N. O'Shea, C. Isvoranu, and J. Schnadt, J. Chem. Phys. **127**, 134707 (2007).
[15] J. Concepcion, J. W. Jurss, M. R. Norris, Z. F. Chen, J. L. Templeton, and T. J. Meyer, Inorg. Chem. **49**, 1277 (2010).
[16] J. Concepcion, J. W. Jurss, J. L. Templeton, and T. J. Meyer, J. Am. Chem. Soc. **49**, 16462 (2008).
[17] J. Concepcion, J. W. Jurss, M. K. Brennaman, P. G. Hoertz, A. O. T. Patrocinio, N. Y. M. Iha, J. L. Templeton, and T. J. Meyer, Acc. Chem. Res. **42**, 1954 (2009).
[18] J. N. O'Shea, J. B. Taylor, J. C. Swarbrick, G. Magnano, L. C. Mayor, and K. Schulte, Nanotechnology **18**, 035707 (2007).
[19] A. Saywell, G. Magnano, C. J. Satterley, L. M. A. Perdigao, N. R. Champness, P. H. Beton, and J. N. O'Shea, J. Phys. Chem. **112**, 7706 (2008).
[20] C. J. Satterley, L. M. A. Perdigao, A. Saywell, G. Magnano, A. Rienzo, L. C. Mayor, V. R. Dhanak, P. H. Beton, and J. N. O'Shea, Nanotechnology **18**, 455304 (2007).
[21] A. Rienzo, L. C. Mayor, G. Magnano, C. J. Satterley, E. Ataman, J. Schnadt, and J. N. O'Shea, J. Chem. Phys. **132**, 084703 (2010).
[22] J. E. Lyon, A. J. Cascio, M. M. Beerborn, R. Schlaf, Y. Zhu, and S. A. Jenekhe, Appl. Phys. Letts. **88**, 222109 (2006).
[23] S. Rauschenbach, F. L. Stadler, E. Lunedei, N. Malinowski, S. Koltsov, G. Costantini, and K. Kern, Small **2**, 540 (2006).
[24] L. C. Mayor, A. Saywell, G. Magnano, C. J. Satterley, J. Schnadt, and J. N. O'Shea, J. Chem. Phys. **130**, 164704 (2009).
[25] R. Nyholm, J. N. Andersen, U. Johansson, B. N. Jensen, and I. Lindau, J. Electron Spectrosc. Relat. Phenom. **467–468**, 520 (2001).
[26] J. Schnadt, J. N. O'Shea, L. Patthey, J. Schiessling, J. Krempaský, M. Shi, J. Schiessling, N. Mårtensson, and P. A. Brühwiler, Surf. Sci. **544**, 74 (2003).
[27] B. Delley, J. Chem. Phys. **92**, 508 (1990).
[28] B. Delley, J. Chem. Phys. **113**, 7756 (2000).
[29] J. P. Perdew, K. Burke, and M. Enzerhof, Phys. Rev. Lett. **77**, 3865 (1996).
[30] J. N. O'Shea, Y. Luo, J. Schnadt, L. Patthey, H. Hillesheimer, J. Krempaský, D. Nordlund, M. Nagasono, and N. Mårtensson, Surf. Sci. **486**, 157 (2001).
[31] J. N. O'Shea, J. Schnadt, P. A. Brühwiler, and H. H. N. Mårtensson, J. Phys. Chem. B **105**, 1917 (2001).
[32] J. N. O'Shea, J. C. Swarbrick, K. Nilson, C. Puglia, B. Brena, Y. Luo, and V. Dhanak, J. Chem. Phys. **121**, 10203 (2004).
[33] J. C. Fuggle and N. Mårtensson, J. Electron Spectrosc. Relat. Phenom. **21**, 275 (1980).
[34] J. Schnadt, J. N. O'Shea, L. Patthey, J. Krempaský, N. Mårtensson, and P. A. Brühwiler, Phys. Rev. B **67**, 235420 (2003).
[35] J. B. Taylor, L. C. Mayor, J. C. Swarbrick, J. N. O'Shea, and J. Schnadt, J. Phys. Chem. C **111**, 16646 (2007).
[36] J. Schnadt, P. A. Brühwiler, L. Patthey, J. N. O'Shea, S. Södergren, M. Odelius, R. Ahuja, O. Karis, M. Bässler, P. Persson, H. Siegbahn, S. Lunell, and N. Mårtensson, Nature **418**, 620 (2002).
[37] J. Schnadt, J. N. O'Shea, L. Patthey, L. Kjeldgaard, J. Åhlund, K. Nilson, J. Schiessling, J. Krempaský, M. Shi, O. Karis, C. Glover, H. Siegbahn, N. Mårtensson, and P. A. Brühwiler, J. Chem. Phys. **119**, 12462 (2003).
[38] P. Persson, S. Lunell, P. A. Brühwiler, J. Schnadt, S. Södergren, J. N. O'Shea, O. Karis, H. Siegbahn, N. Mårtensson, M. Bässler, and L. Patthey, J. Chem. Phys. **112**, 3945 (2000).
[39] J. N. O'Shea, J. B. Taylor, L. C. Mayor, J. C. Swarbrick, and J. Schnadt, Surf. Sci. **602**, 1693 (2008).
[40] J. Schnadt, J. Schiessling, and P. A. Brühwiler, Chem. Phys. **312**, 39 (2005).
[41] P. A. Brühwiler, O. Karis, and N. Mårtensson, Rev. Mod. Phys. **74**, 703 (2002).
[42] B. Kempgens, A. Kivimaki, M. Neeb, H. M. Koppe, A. M. Bradshaw, and J. Feldhaus, J. Phys. B. **29**, 5389 (1996).
[43] R. J. Ellingson, J. B. Asbury, S. Ferrere, H. N. Ghosh, J. R. Sprague, T. Q. Lian, and A. J. Nozik, J. Phys. Chem. B. **102**, 34 (1998).
[44] J. B. Asbury, R. J. Ellingson, H. N. Ghosh, S. Ferrere, A. J. Nozik, and T. Q. Lian, J. Phys. Chem. B. **103**, 3110 (1999).
[45] P. Persson and M. J. Lundqvist, J. Phys. Chem. B. **109**, 11918 (2005).
[46] K. Westermark, H. Rensmo, J. Schnadt, P. Persson, S. Södergren, P. A. Brühwiler, S. Lunell, and H. Siegbahn, Chem. Phys. **285**, 167 (2002).
[47] J. A. D. Matthew and Y. Komninos, Surf. Sci. **53**, 716 (1975).